SUPPLEMENTAL DATA

Inventory:

Figure S1

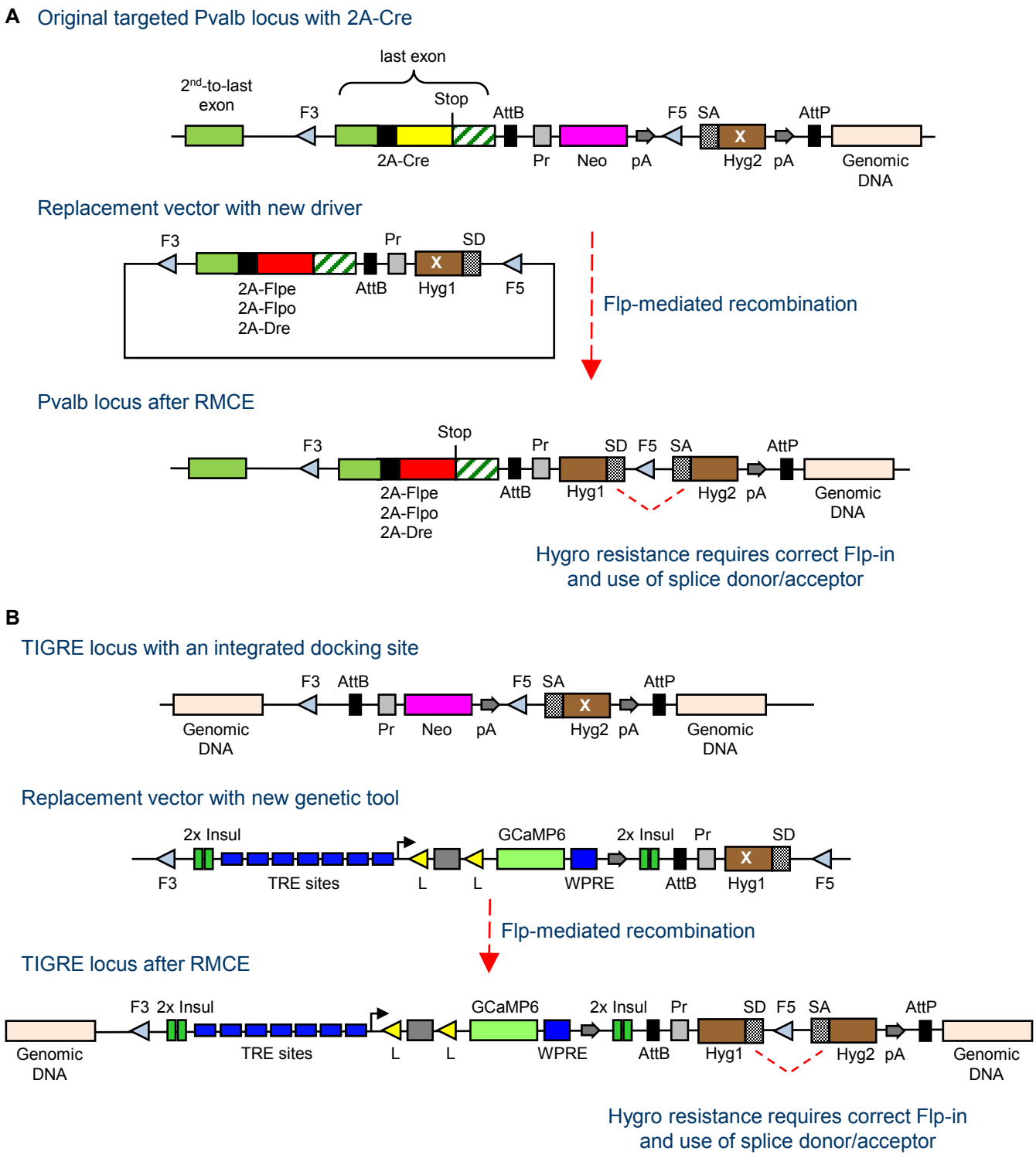
A
Original targeted Pvalb locus with 2A-Cre
last exon
2nd-to-last exon
Stop
F3
AttB
F5
SA
AttP
2A-Cre
Pr
Neo
pA
X
Hyg2
pA
Genomic DNA
Replacement vector with new driver
F3
Pr
SD
2A-Flpe
2A-Flpo
2A-Dre
AttB
Hyg1
F5
Flp-mediated recombination
Pvalb locus after RMCE
Stop
F3
Pr
SD
F5
SA
AttP
2A-Flpe
2A-Flpo
2A-Dre
AttB
Hyg1
Hyg2
pA
Genomic DNA
Hygro resistance requires correct Flp-in and use of splice donor/acceptor
B
TIGRE locus with an integrated docking site
F3
AttB
F5
SA
AttP
Genomic DNA
Pr
Neo
pA
X
Hyg2
pA
Genomic DNA
Replacement vector with new genetic tool
2x Insul
GCaMP6
2x Insul
Pr
SD
F3
TRE sites
L
L
WPRE
AttB
Hyg1
F5
Flp-mediated recombination
TIGRE locus after RMCE
F3
2x Insul
GCaMP6
2x Insul
Pr
SD
F5
SA
AttP
Genomic DNA
TRE sites
L
L
WPRE
AttB
Hyg1
Hyg2
pA
Genomic DNA
Hygro resistance requires correct Flp-in and use of splice donor/acceptor

Figure S1. Recombinase-mediated cassette exchange (RMCE) strategy for inserting new transgenes into the *Pvalb* locus or the TIGRE locus. (Related to **Figures 1** and **3**.) Our RMCE strategy is based on Flp-mediated recombination of FRT3 (F3) and FRT5 (F5) target sites, thus the process is also called "Flp-in". (**A**) RMCE in the *Pvalb* locus. The *Pvalb* locus was originally targeted by homologous recombination to insert T2A-Cre at the endogenous stop codon (top). This ES clone was used in subsequent RMCE experiments to replace T2A-Cre with other driver gene cassettes, including T2A-Flpe, T2A-Flpo, or T2A-Dre. To do this, the originally targeted Pvalb-2A-Cre ES clone is co-transfected with a Flp expression plasmid and a replacement vector containing the modified exon with the new driver (middle). F3 and F5 sites are incompatible with each other, so there is no recombination between them. In the presence of Flp, F3 and F5 each undergoes homophilic recombination, *i.e.* between the F3 (or F5) in the genomic locus and the F3 (or F5) in the replacement vector, leading to the replacement of the DNA segment between F3 and F5 in the genomic locus with that from the replacement vector. Successful cassette exchange joins Hyg1 and Hyg2 domains through mRNA splicing and reconstitutes an active hygromycin-resistant gene, which can be used for selection of exchange events. Since all of our in-house gene targeting experiments utilize the same targeting vector design shown here, *Pvalb*-like RMCE approach is applicable to other targeted gene loci as well, such as the *Snap25* locus reported here. (**B**) RMCE in the TIGRE locus. The originally targeted TIGRE ES clone, containing a Flp/FRT-based empty docking site integrated into the TIGRE locus (top), is co-transfected with a Flp expression plasmid and a replacement vector containing the transgene cassette of interest (middle). The Flp-in RMCE process is identical to that described in A.

Figure S2

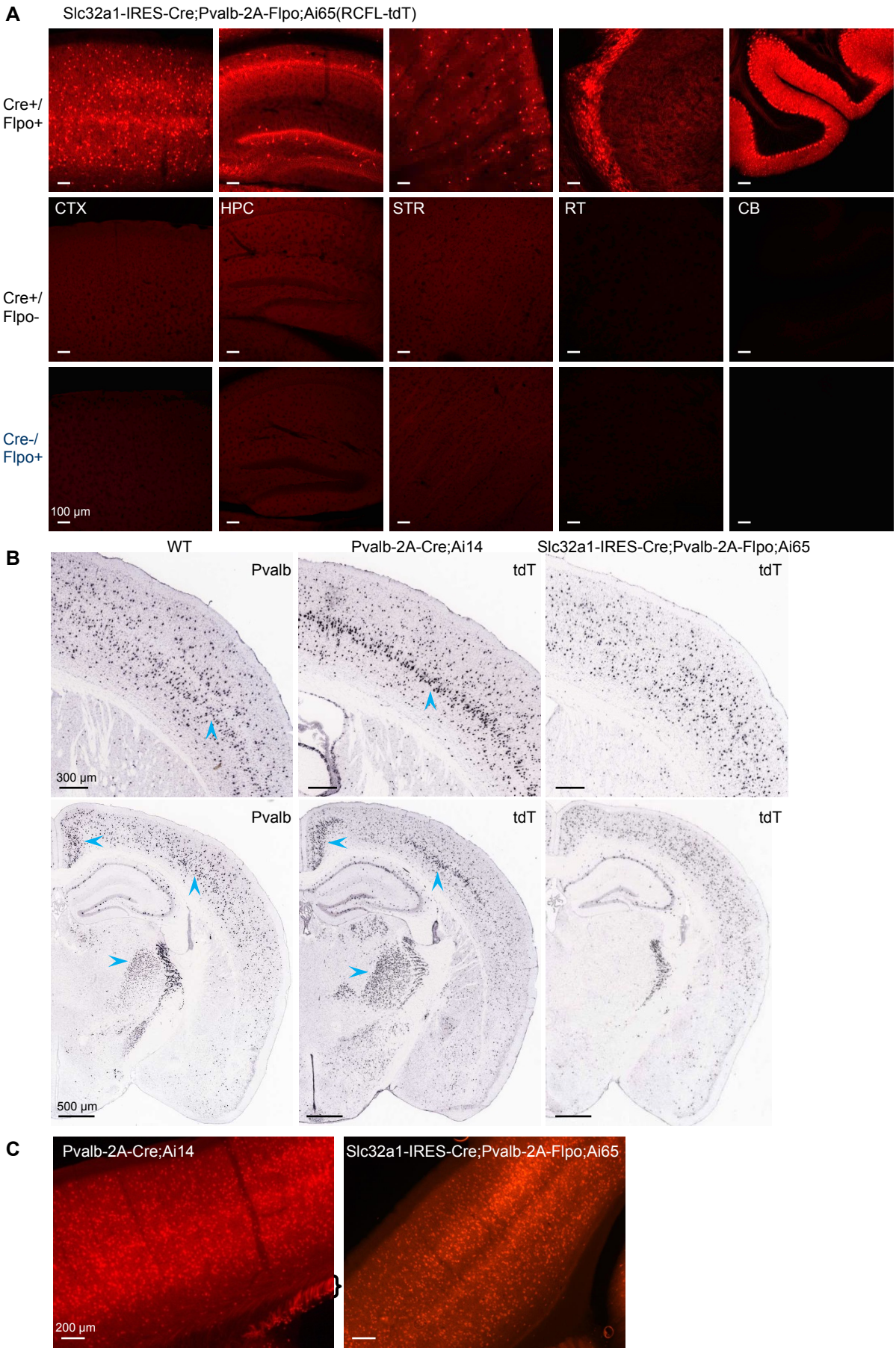
A
Slc32a1-IRES-Cre;Pvalb-2A-Flpo;Ai65(RCFL-tdT)
Cre+/
Flpo+
CTX
HPC
STR
RT
CB
Cre+/
Flpo-
Cre-/
Flpo+
100 μm
B
WT
Pvalb-2A-Cre;Ai14
Slc32a1-IRES-Cre;Pvalb-2A-Flpo;Ai65
Pvalb
tdT
tdT
300 μm
Pvalb
tdT
tdT
500 μm
C
Pvalb-2A-Cre;Ai14
Slc32a1-IRES-Cre;Pvalb-2A-Flpo;Ai65
200 μm

Figure S2. Dual-recombinase intersection using Cre and Flp. (Related to **Figure 1**.) (**A**) Confocal images show that expression of tdTomato reporter in *Slc32a1*+/*Pvalb*+ GABAergic neurons of the Slc32a1-IRES-Cre;Pvalb-2A-Flpo;Ai65 mouse requires both Cre and Flp recombinases. No tdTomato+ cells were found in either Cre+/Flp- or Cre-/Flp+ mouse. CTX, cortex. HPC, hippocampus. STR, striatum. RT, reticular nucleus of the thalamus. CB, cerebellum. (**B**) ISH images comparing the expression pattern of the endogenous *Pvalb* gene with that of the tdTomato reporter gene in the Pvalb-2A-Cre;Ai14 mouse or the Slc32a1-IRES-Cre;Pvalb-2A-Flpo;Ai65 mouse. The endogenous *Pvalb* gene is not only expressed prominently in GABAergic neurons but also at lower levels in excitatory neurons in different parts of the brain, including cortical layer 5 and some nuclei of the thalamus (blue arrow heads, left panels). Consequently, tdTomato reporter is also expressed in these non-GABAergic neurons in the Pvalb-2A-Cre;Ai14 mouse (blue arrow heads, middle panels). No expression in excitatory neurons is observed in the Slc32a1-IRES-Cre;Pvalb-2A-Flpo;Ai65 mouse (right panels). WT, wild-type mouse. (**C**) The presence of cortical excitatory neurons in the Pvalb-2A-Cre;Ai14 mouse can be confirmed by the presence of labeled axon bundles in the white matter, as indicated by the bracket in the left panel. No labeled axon bundles were found in the white matter beneath the cortex in the Slc32a1-IRES-Cre;Pvalb-2A-Flpo;Ai65 mouse (right panel).

Figure S3

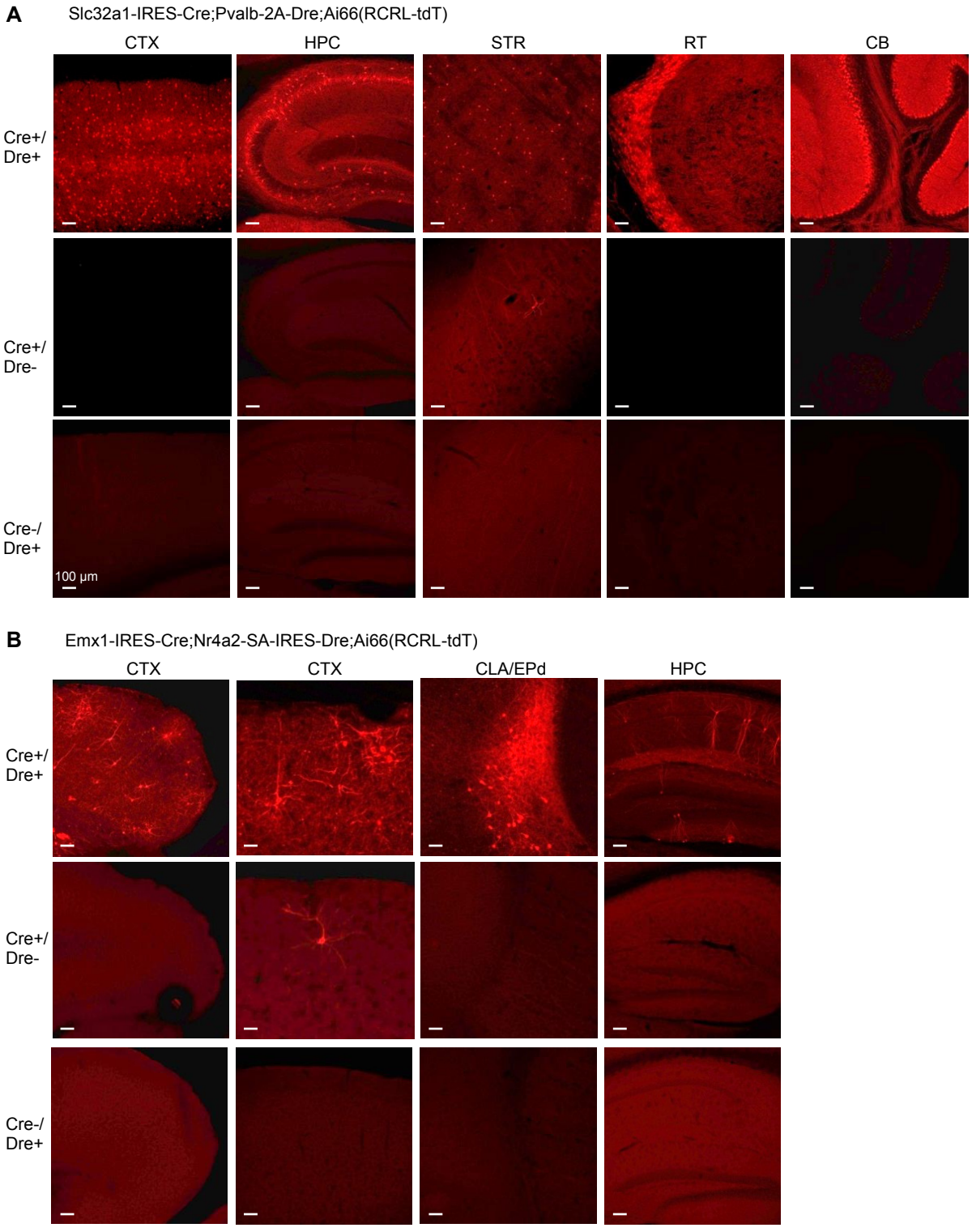
A
Slc32a1-IRES-Cre;Pvalb-2A-Dre;Ai66(RCRL-tdT)
CTX
HPC
STR
RT
CB
Cre+/
Dre+
Cre+/
Dre-
Cre-/
Dre+
100 µm
B
Emx1-IRES-Cre;Nr4a2-SA-IRES-Dre;Ai66(RCRL-tdT)
CTX
CTX
CLA/EPd
HPC
Cre+/
Dre+
Cre+/
Dre-
Cre-/
Dre+

Figure S3. Dual-recombinase intersection using Cre and Dre. (Related to **Figure 1**.) (**A**) Confocal images show that expression of tdTomato reporter in *Slc32a1*+/*Pvalb*+ GABAergic neurons of the Slc32a1-IRES-Cre;Pvalb-2A-Dre;Ai66 mouse requires both Cre and Dre recombinases. Only a couple of tdTomato+ cells were seen in the striatum of Cre+/Dre- mouse. No tdTomato+ cells were found in Cre-/Dre+ mouse. CTX, cortex. HPC, hippocampus. STR, striatum. RT, reticular nucleus of the thalamus. CB, cerebellum. (**B**) Confocal images show that expression of tdTomato reporter in the Emx1-IRES-Cre;Nr4a2-SA-IRES-Dre;Ai66 mouse is restricted to the *Emx1*+/*Nr4a2*+ neurons in the claustrum (CLA) and endopiriform nucleus, dorsal part (EPd), as well as sparsely scattered cells in cortex (CTX) and hippocampus (HPC), where both Cre and Dre are present. No tdTomato+ cells were found in the Cre-/Dre+ mouse. However, a few tdTomato+ cells were found in the Cre+/Dre- mouse, indicating a very low level of promiscuity of Cre activity for recombining the Rox sites.

Figure S4

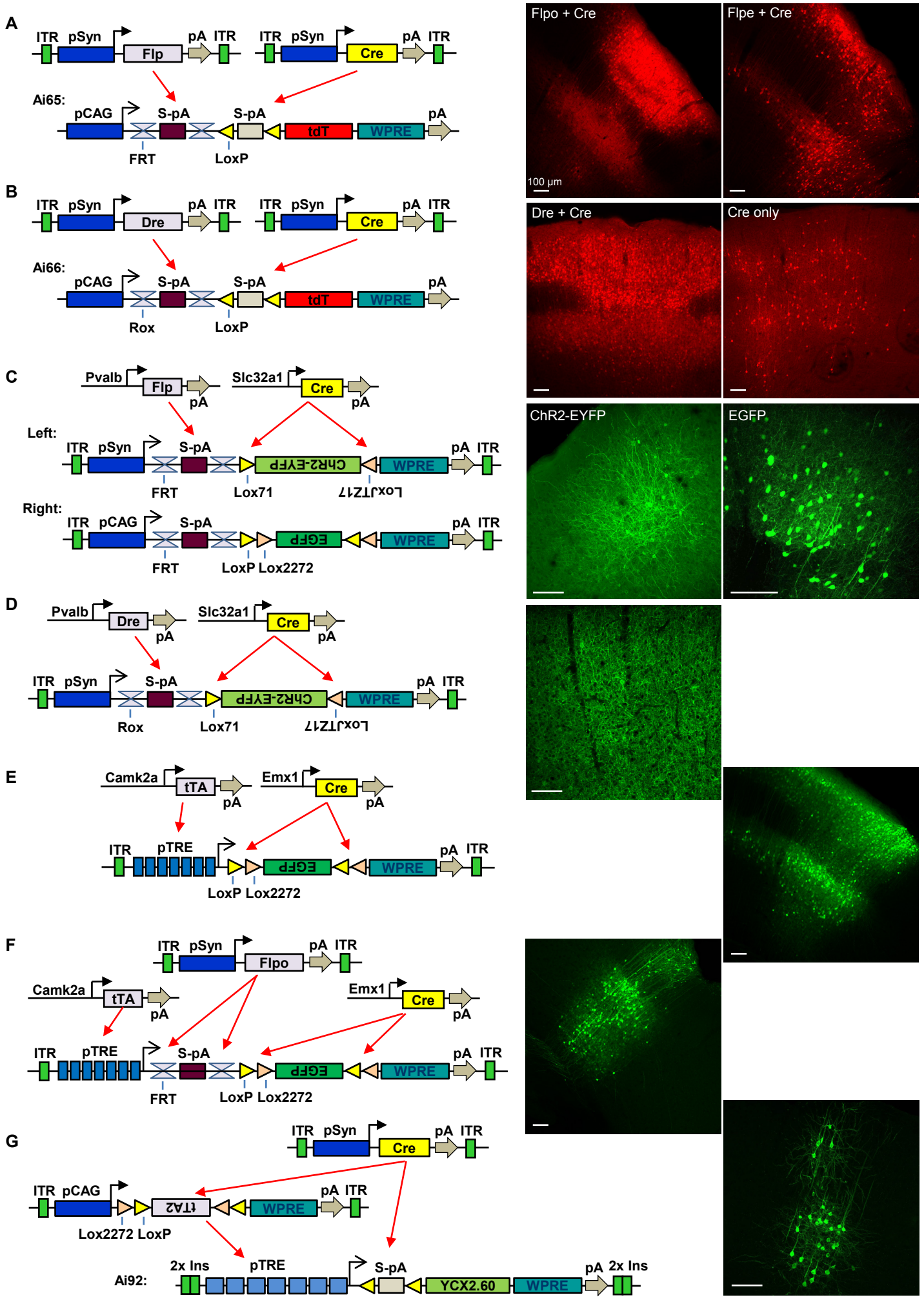
A
ITR pSyn Flp pA ITR
ITR pSyn Cre pA ITR
Ai65:
pCAG S-pA S-pA tdT WPRE pA
FRT LoxP
B
ITR pSyn Dre pA ITR
ITR pSyn Cre pA ITR
Ai66:
pCAG S-pA S-pA tdT WPRE pA
Rox LoxP
C
Pvalb Flp pA
Slc32a1 Cre pA
Left:
ITR pSyn S-pA ChR2-EYFP WPRE pA ITR
FRT Lox71 Lox71
Right:
ITR pCAG S-pA EGFP WPRE pA ITR
FRT LoxP Lox2272
D
Pvalb Dre pA
Slc32a1 Cre pA
ITR pSyn S-pA ChR2-EYFP WPRE pA ITR
Rox Lox71 Lox71
E
Camk2a tTA pA
Emx1 Cre pA
ITR pTRE EGFP WPRE pA ITR
LoxP Lox2272
F
ITR pSyn Flpo pA ITR
Camk2a tTA pA
Emx1 Cre pA
ITR pTRE S-pA EGFP WPRE pA ITR
FRT LoxP Lox2272
G
ITR pSyn Cre pA ITR
ITR pCAG tTA2 WPRE pA ITR
Lox2272 LoxP
Ai92:
2x Ins pTRE S-pA YCX2.60 WPRE pA 2x Ins
Flpo + Cre
Flpe + Cre
100 µm
Dre + Cre
Cre only
ChR2-EYFP
EGFP

Figure S4. New recombinant adeno-associated viruses (AAVs) for intersectional strategies. (Related to **Figures 1** and **2**.) (**A-B**) We developed AAVs expressing Cre, Flpe, Flpo or Dre under the Synapsin I promoter (**Table 1**). (**A**) Coinjection of AAV-Cre and AAV-Flpe, or AAV-Cre and AAV-Flpo into Ai65(RCFL-tdT) mice resulted in efficient recombination with AAV-Cre and AAV-Flpo, but with much lower efficiency with AAV-Cre and AAV-Flpe. Single-virus injections of AAV-Cre, AAV-Flpe or AAV-Flpo into Ai65(RCFL-tdT) mice gave no tdT+ cells (data not shown). (**B**) Coinjection of AAV-Cre and AAV-Dre into Ai66(RCRL-tdT) mice resulted in efficient recombination. Single injection of AAV-Cre into Ai66(RCRL-tdT) mice exhibited sparse promiscuous recombination. Single injection of AAV-Dre into Ai66(RCFL-tdT) mice gave no tdT+ cells (data not shown). (**C**) Injection of the Cre/Flp double reporter AAV, phSyn1-FSF-FLEX-ChR2(H134R)-EYFP-WPRE-bGHpA (left image) or pCAG-FSF-FLEX-EGFP-WPRE-bGHpA (right image), into the Slc32a1-IRES-Cre;Pvalb-2A-Flpo double driver mouse resulted in labeling of *Slc32a1*+/*Pvalb*+ interneurons. (**D**) Injection of the Cre/Dre double reporter AAV, phSyn1-RSR-FLEX-ChR2(H134R)-EYFP-WPRE-bGHpA, into the Slc32a1-IRES-Cre;Pvalb-2A-Dre double driver mouse resulted in membrane EYFP labeling of *Slc32a1*+/*Pvalb*+ interneurons. (**E**) Injection of the Cre/tTA double reporter AAV, pTRE-FLEX-EGFP-WPRE-bGHpA, into the Emx1-IRES-Cre;Camk2a-tTA double driver mouse resulted in cytoplasmic EGFP labeling of cortical neurons. (**F**) Coinjection of the Cre/Flp/tTA triple reporter AAV, pTRE-FSF-FLEX-EGFP-WPRE-bGHpA, with AAV-Flpo into the Emx1-IRES-Cre;Camk2a-tTA double driver mouse resulted in cytoplasmic EGFP labeling of cortical neurons. (**G**) Coinjection of AAV-Cre and AAV pCAG-FLEX2-tTA2-WPRE-bGHpA into Ai92(TITL-YCX2.60) mouse resulted in robust expression of YCX2.60 in cortical neurons.

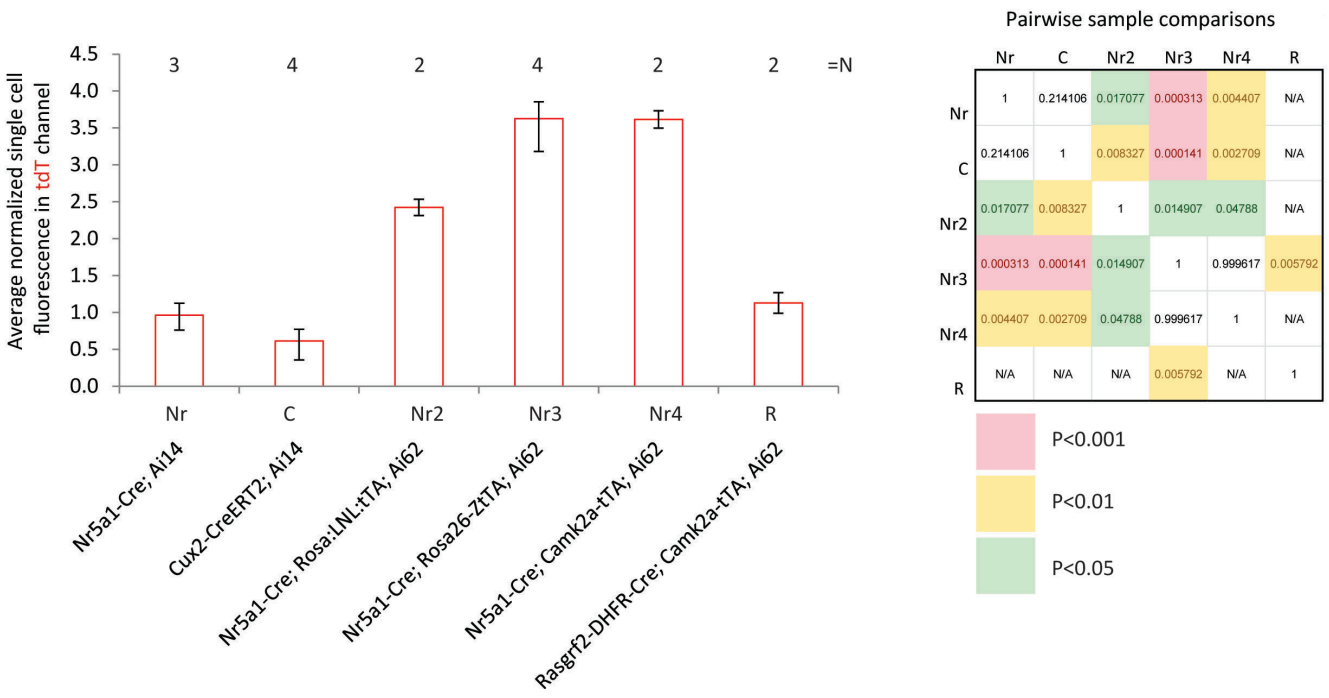

Figure S5. Comparison of average tdTomato reporter expression in individual neurons isolated from different transgenic mice by fluorescence-activated cell sorting (FACS). (Related to **Figure 2**.) Nr5a1-Cre selectively labels cortical layer 4 neurons, Cux2-CreERT2 labels cortical layer 2/3 and 4 neurons, and Rasgrf2-2A-dCre preferentially labels cortical layer 2/3 neurons. Sorting was performed on a BD FACSAriaII SORP with DAPI added to single cell suspension to detect dead cells. The FACS populations analyzed were chosen to include single cells with low DAPI and high tdTomato fluorescence. To correct for the day-to-day differences in laser power, the cellular fluorescence readouts were normalized by signal obtained daily from fluorescent beads (BD Quantibrite PE Beads, BD Biosciences) analyzed using the same laser power settings in the same channel. Subsequently, to simplify comparisons, all average fluorescence values were divided by the average fluorescence for Nr5a1-Cre;Ai14 cells (thereby set at 1). Number of individual replicates (N) for each genotype is shown on top; error bars represent range. Group medians show statistically significant overall variation (Kruskal-Wallis test; chi-squared = 14.7487, df = 5, p = 0.01149). Post-hoc comparisons by Games-Howell test on the left highlight statistically significant pairwise differences (presented as a heatmap of p values; N/A represents pairs in which combined N < 5, and for which the test cannot be applied).

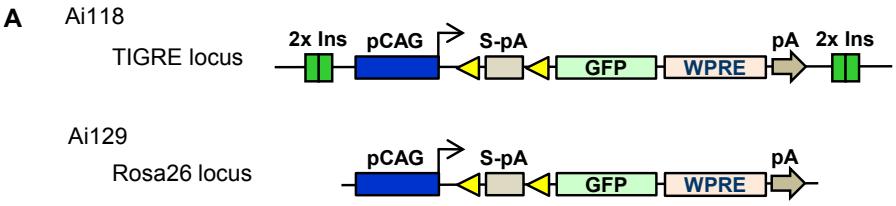

B FACS analysis of clones after transient transfection with CMV-Cre

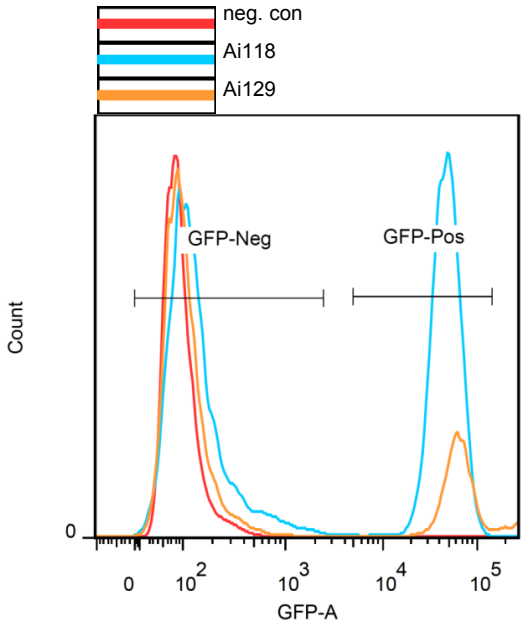

	Mean GFP-	Mean GFP+
Neg. control	91.4	n/a
Ai118,1	173	4.66E4
Ai118,2	154	4.35E4
Ai129,1	112	6.12E4
Ai129,2	165	5.85E4

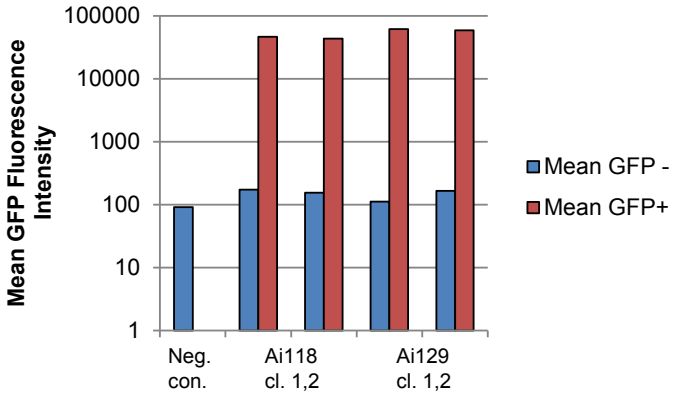

C Sorted GFP+ cells after transient CMV-Cre transfection

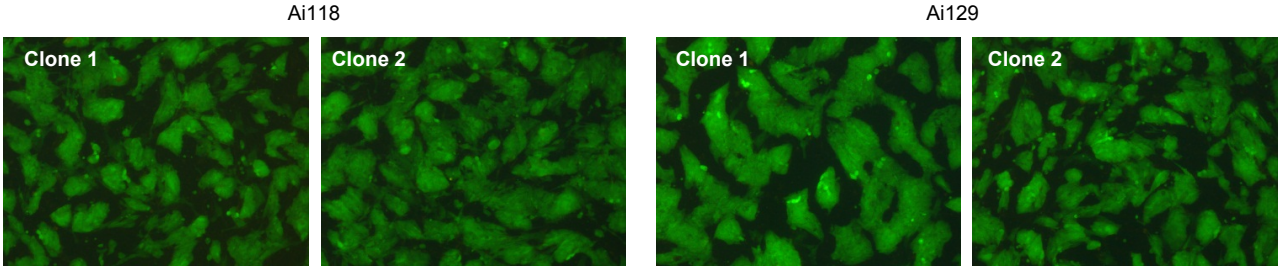

Figure S6. Comparison of EGFP expression in ES clones carrying a pCAG-LSL-EGFP cassette targeted to either the TIGRE locus (Ai118 clones) or the Rosa26 locus (Ai129 clones). (Related to **Figure 2**.) (**A**) Configuration of the two types of targeted ES clones under comparison. (**B**) Transient transfection of 2 independent ES clones from each of Ai118 or Ai129 with a pCMV-Cre plasmid turns on EGFP expression in a portion of the ES cells. FACS analysis of the transfected cells showed two peaks, corresponding to non-Cre-activated EGFP-negative cells and Cre-activated EGFP-positive cells. Comparable GFP fluorescence levels were observed between EGFP+ cells in the Ai118 and Ai129 populations, with Ai129 fluorescence being approximately 30% higher. (**C**) Sorted EGFP+ cells were re-plated and grown in dishes, and they exhibited comparable levels of EGFP fluorescence under the microscope.

Figure S7

A

Emx1-IRES-Cre;Ai35, P147, n=2

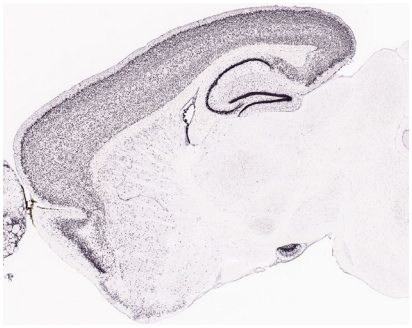

Emx1-IRES-Cre;Ai57(RCL-Jaws), P122, n=2

Emx1-IRES-Cre;Camk2a-tTA;Ai79(TITL-Jaws), P330, n=3

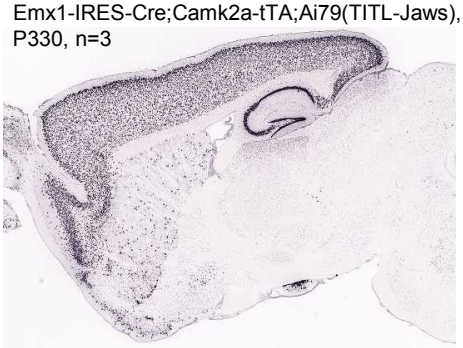

Emx1-IRES-Cre;Camk2a-tTA;Ai62(TITL-tdT), P57, n=2

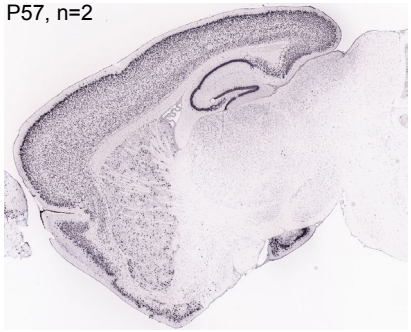

Emx1-IRES-Cre;Ai95(RCL-GCaMP6f), P147, n=1

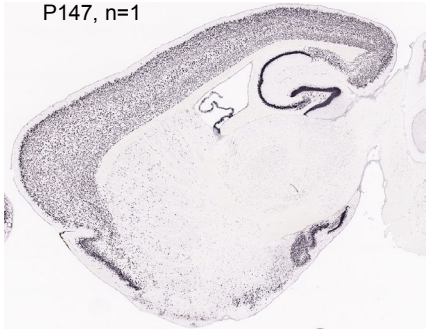

Emx1-IRES-Cre;Camk2a-tTA;Ai93(TITL-GCaMP6f), P112, n=2

Emx1-IRES-Cre;Ai87(RCL-iGluSnFR), P57, n=1

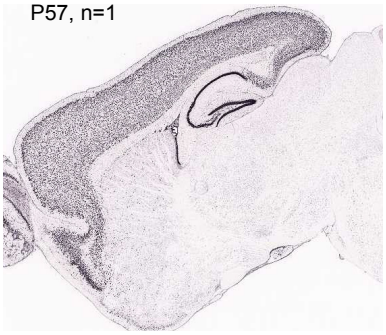

Emx1-IRES-Cre;Camk2a-tTA;Ai85(TITL-iGluSnFR), P56 & P185, n=2

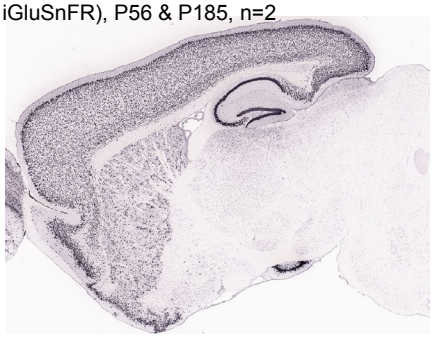

Emx1-IRES-Cre;ROSA26-ZtTA;Ai78(TITL-VSFPB), P76, n=2

B

Rasgrf2-2A-dCre;Ai14, P56, n=2

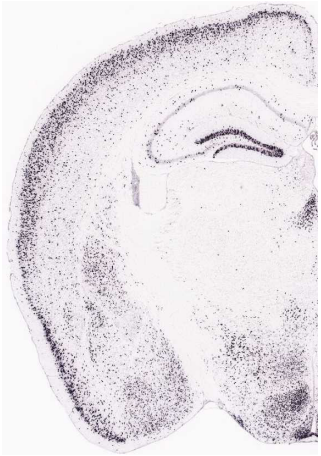

Rasgrf2-2A-dCre;Camk2a-tTA; Ai78(TITL-VSFPB), P167, n=1

C

Gad2-IRES-Cre;Ai14, P56, n=5

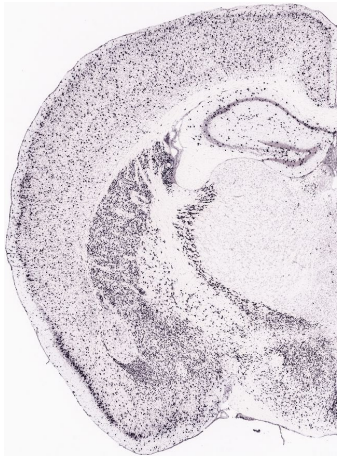

Gad2-IRES-Cre;ROSA26-ZtTA; Ai92(TITL-YCX2.60), P102, n=2

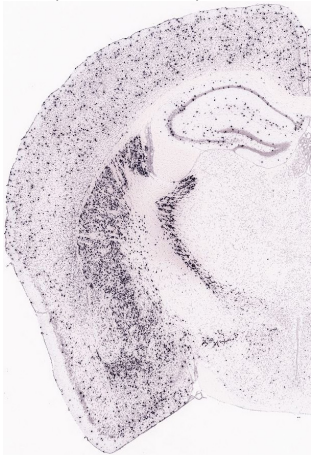

D

Chat-IRES-Cre;ROSA26-ZtTA;Ai93(TITL-GCaMP6f), P95, n=2

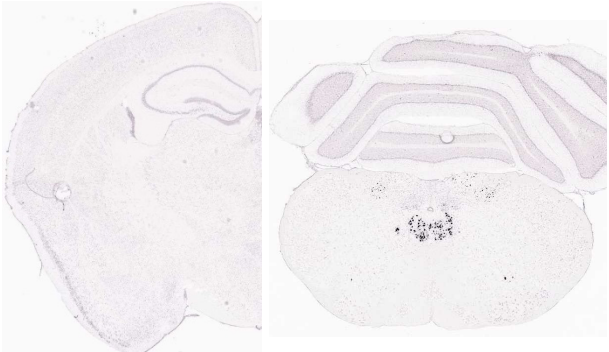

E

Snap25-2A-GCaMP6s, P185, n=4

Figure S7. Reporter gene expression patterns in multiple transgenic lines by *in situ* hybridization (ISH). (Related to **Figure 4**.) Number of mice used for ISH for each line and their representative age are shown. EYFP riboprobe was used in all cases except for Ai14 and Ai62 containing specimens in which tdTomato riboprobe was used. Note that expression levels can't be compared reliably between different mice due to the saturation of ISH signals in all three expression systems: Rosa-CAG, TIGRE-TRE and Snap25. (**A**) ISH comparison of various Rosa26 and TIGRE lines under the control of Emx1-IRES-Cre alone, or in combination with Camk2a-tTA or ROSA26-ZtTA. All mice exhibited widespread and high-density expression in cortex, and there was no significant difference in number of expressed cells between different lines or across ages. There is variability in number of expressed cells in striatum. (**B**) ISH comparison between Rosa26 and TIGRE lines under the control of Rasgrf2-2A-dCre alone or in combination with Camk2a-tTA. (**C**) ISH comparison between Rosa26 and TIGRE lines under the control of Gad2-IRES-Cre alone or in combination with ROSA26-ZtTA. In the Gad2-IRES-Cre;ROSA26-ZtTA;Ai92(TITL-YCX2.60) mice, the numbers of expressed cells were moderately reduced in cortex, but substantially reduced in selected subcortical regions. (**D**) In Chat-IRES-Cre;ROSA26-ZtTA;Ai93(TITL-GCaMP6f) mice, there was no detectable reporter gene expression in basal forebrain cholinergic neurons (left panel), although reporter gene was expressed in brainstem cholinergic neurons (right panel). (**E**) Widespread transgene expression throughout the brain in Snap25-2A-GCaMP6s mice.

Figure S8

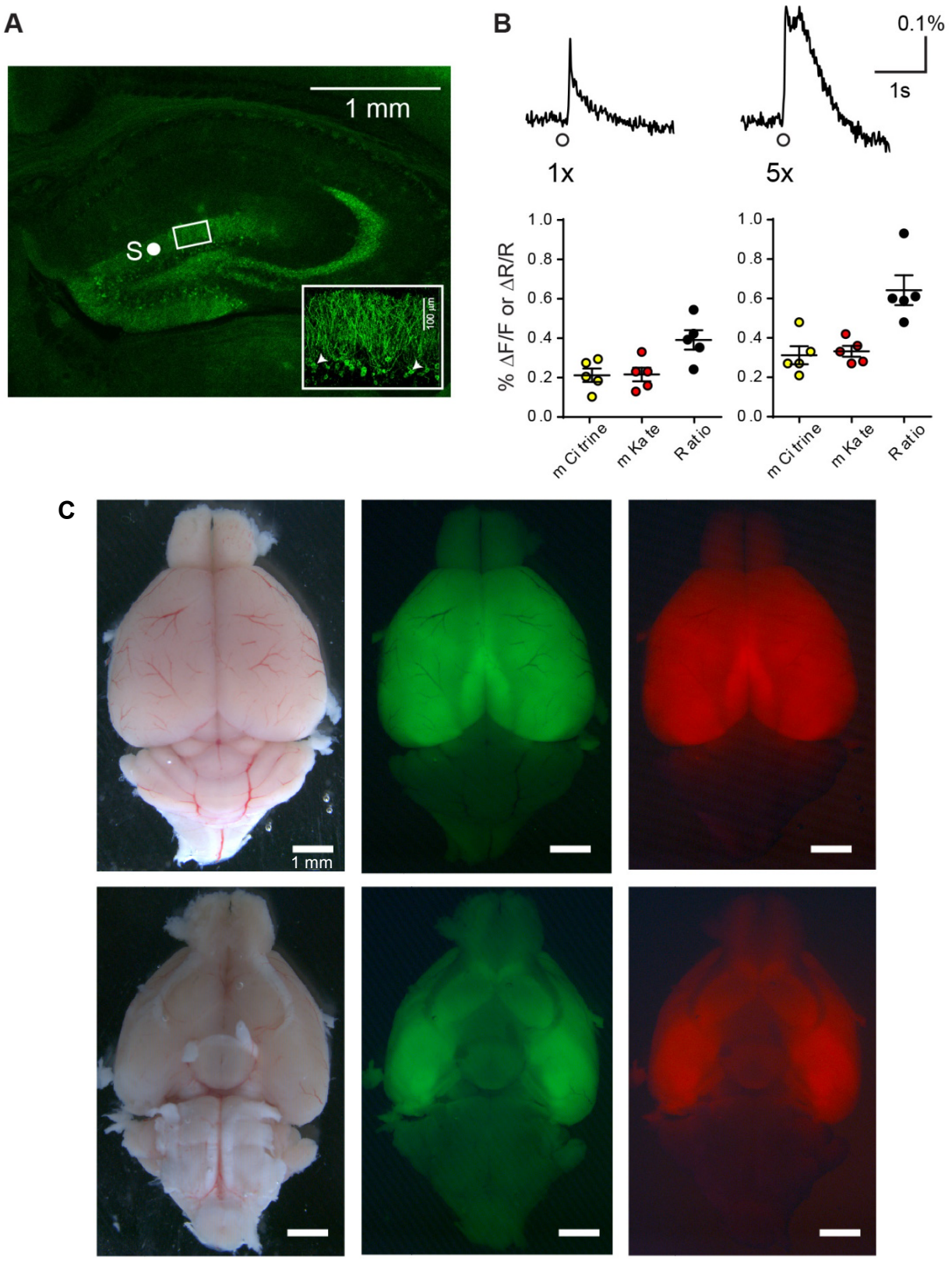
A
1 mm
S
100 μm
B
0.1%
1s
1x
5x
% ΔF/F or ΔR/R
1.0
0.8
0.6
0.4
0.2
0.0
mCitrine
mKate
Ratio
C
1 mm

Figure S8. Functional reporting of population responses from the hippocampus in Rasgrf2-2A-dCre; Camk2a-tTA;Ai78(TITL-VSFPB) mice. (Related to **Figure 5**.) (**A**) Expression of VSFP-Butterfly 1.2 (green) in the dentate gyrus, consistent with expression in granule cells (GCs), inset, examples denoted by arrowheads. (**B**) In 300-µm coronal slices containing the hippocampus, perforant path stimulation (20V at point S, in A) evoked VSFP responses from GC dendrites (rectangular region of interest in A) coincident with field EPSPs (not shown). Repetitive 5x stimulation (100 Hz) evoked larger and longer responses. Traces in upper panels from a single slice, and black symbols in lower panels, are ratios (% ΔR/R) of decreased mCitrine fluorescence (% -ΔF/F, yellow symbols) and increased mKate2 fluorescence (% ΔF/F, red symbols), for 5 recordings from five 2-3 months old mice. Traces are an average of 3 sweeps. Scale bar is 0.1% change in ratio and 1 second, sampling at 100Hz. (**C**) A freshly dissected mouse brain showing the evenness of mCitrine (green) and mKate2 (red) fluorescence of VSFP-Butterfly 1.2 throughout the cortex.

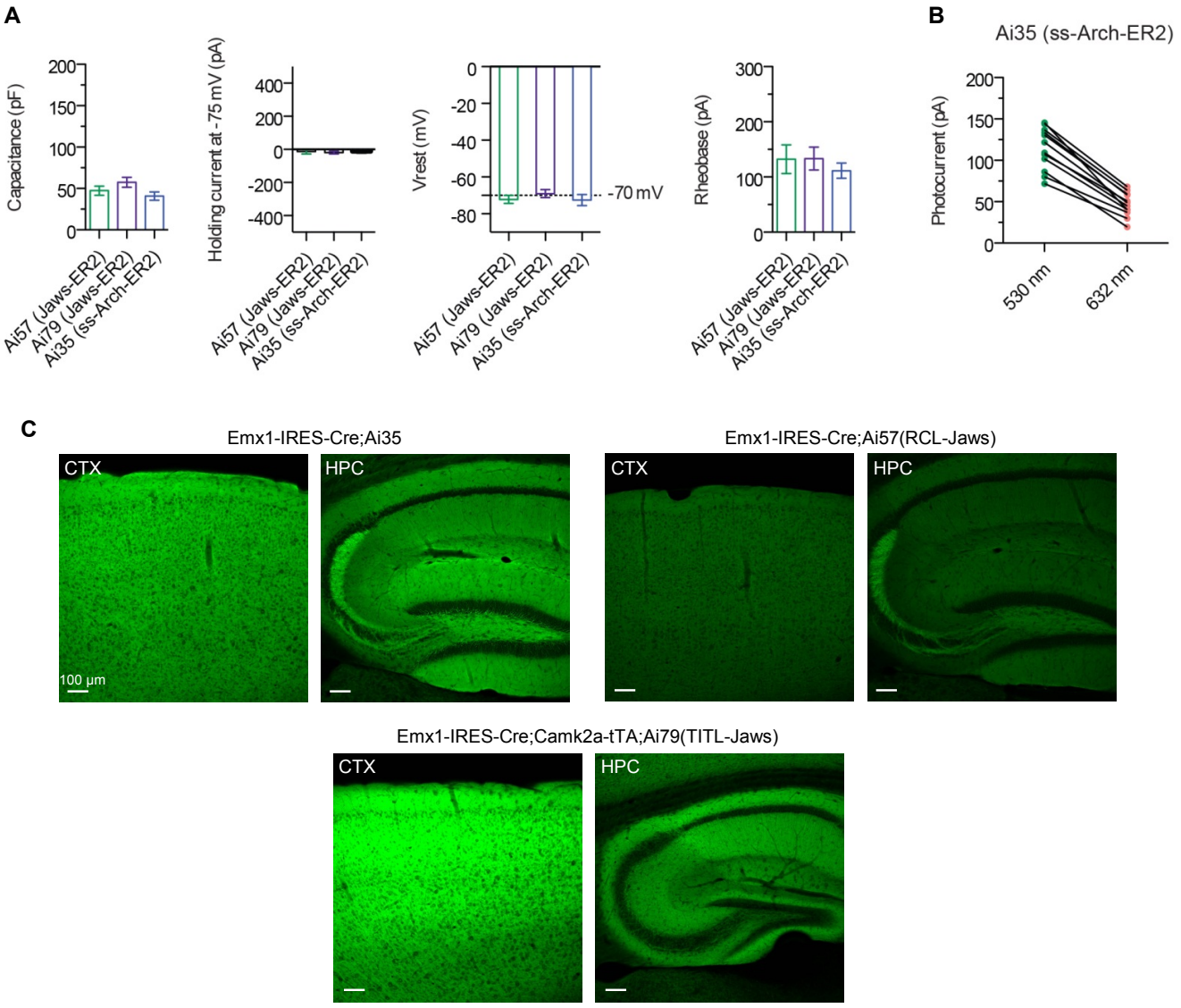

Figure S9. Comparison of expression levels and membrane properties for Emx1-IRES-Cre;Ai57(RCL-Jaws) mice (simplified as Ai57), Emx1-IRES-Cre;Camk2a-tTA;Ai79(TITL-Jaws) mice (simplified as Ai79), and Emx1-IRES-Cre;Ai35 mice (simplified as Ai35). (Related to **Figure 8**.) (**A**) Normal membrane electrophysiological properties in Jaws-expressing neurons in brain slices from Ai57, Ai79 and Ai35 mice. All values represent mean ± SEM. (**B**) Comparison of red or green light (632 or 530 nm; 5 mW/mm^2) induced photocurrents in slices from Ai35 mice. (**C**) Compared to Rosa-CAG based reporter Ai35 which expresses Arch-GFP-ER2, the Rosa-CAG based reporter Ai57 shows weaker fluorescence for Jaws-GFP-ER2, whereas the TIGRE based reporter Ai79 (when combined with Camk2a-tTA) shows stronger fluorescence for Jaws-GFP-ER2. Confocal images were collected at the same time under the same conditions.

Table S1. Transgenic mouse lines used in this study.

Drivers	**Originating Lab**	**Description**	**Repository Stock #**	**Official Strain Name**
Camk2a-tTA	Mark Mayford	Random insertion: pCamk2a-tTA	JAX 007004	B6.Cg-Tg(Camk2a-tTA)1Mmay/DboJ
Chat-IRES-Cre	Brad Lowell	Knock-into 3' UTR: IRES-Cre	JAX 006410	B6;129S6-Chattm2(cre)Lowl/J
Cux2-CreERT2	Ulrich Mueller	Knock-into ATG: CreERT2	MMRRC 032779	B6(Cg)-Cux2tm3.1(cre/ERT2)Mull/Mmmh
Emx1-IRES-Cre	Kevin Jones	Knock-into 3' UTR: IRES-Cre	JAX 005628	B6.129S2-Emx1tm1(cre)Krj/J
Gad2-IRES-Cre	Z. Josh Huang	Knock-into 3' UTR: IRES-Cre	JAX 010802	STOCK Gad2tm2(cre)Zjh/J
Nr4a2-SA-IRES-Dre	Andras Nagy	Knock-into intron: SA-IRES-Dre		
Nr5a1-Cre	Brad Lowell	Random insertion pNr5a1-Cre	JAX 006364	FVB-Tg(Nr5a1-cre)2Lowl/J
Nxph4-2A-CreERT2	AIBS[a]	Knock-into 3' UTR: T2A-CreERT2	JAX 022861	B6.Cg-Nxph4tm1.1(cre/ERT2)Hze/J
Pvalb-2A-Cre	AIBS	Knock-into 3' UTR: T2A-Cre	JAX 012358	B6.Cg-Pvalbtm1.1(cre)Aibs/J
Pvalb-2A-Dre	AIBS	Knock-into 3' UTR: T2A-DreO	JAX 021190	B6.Cg-Pvalbtm3.1(dreo)Hze/J
Pvalb-2A-Flpo	AIBS	Knock-into 3' UTR: T2A-Flpo	JAX 022730	B6.Cg-Pvalbtm4.1(FLPo)Hze/J
Rasgrf2-2A-dCre	AIBS	Knock-into 3' UTR: T2A-DHFR-Cre	JAX 022864	B6;129S-Rasgrf2tm1(cre/folA)Hze/J
ROSA26-PhiC31	Philippe Soriano	Knock-into intron: SA-PhiC31o-pA-PGKneopA	JAX 007743	B6.129S4-Gt(ROSA)26Sortm3(phiC31*)Sor/J
ROSA:LNL:tTA	Raymond Roos	Knock-in 3' to promoter: loxP-Neo-Stop-loxP-mtTA	JAX 011008	B6.129P2(Cg)-Gt(ROSA)26Sortm1(tTA)Roos/J
ROSA26-ZtTA	Liqun Luo	Knock-into intron: pCA-loxP-β-geo-Stop-loxP-tTA	JAX 012266	STOCK Gt(ROSA)26Sortm5(ACTB-tTA)Luo/J
Scnn1a-Tg3-Cre	AIBS	Random insertion of BAC transgenic at ATG: Cre	JAX 009613	B6;C3-Tg(Scnn1a-cre)3Aibs/J
Slc32a1-IRES-Cre	Brad Lowell	Knock-into 3' UTR: IRES-Cre	JAX 016962	STOCK Slc32a1tm2(cre)Lowl/J
Trib2-2A-CreERT2	AIBS	Knock-into exon 2: F2A-CreERT2	JAX 022865	B6.Cg-Trib2tm1.1(cre/ERT2)Hze/J
Reporters	**Genomic Target**	**Reporter Design**	**Repository Stock #**	**Official Strain Name**
Ai14	Rosa26	pCAG-LSL-tdTomato-WPRE-bGHpA	JAX 007914	B6.Cg-Gt(ROSA)26Sortm14(CAG-tdTomato)Hze/J
Ai35	Rosa26	pCAG-LSL-ss-Arch-GFP-ER2-WPRE-bGHpA	JAX 012735	B6;129S-Gt(ROSA)26Sortm35.1(CAG-aop3/GFP)Hze/J
Ai62(TITL-tdT)	TIGRE	pTRE-LSL-tdTomato-WPRE-bGHpA	JAX 022731	B6.Cg-Igs7tm62.1(tetO-tdTomato)Hze/J
Ai65(RCFL-tdT)	Rosa26	pCAG-FSF-LSL-tdTomato-WPRE-bGHpA	JAX 021875	B6;129S-Gt(ROSA)26Sortm65.1(CAG-tdTomato)Hze/J
Ai66(RCRL-tdT)	Rosa26	pCAG-RSR-LSL-tdTomato-WPRE-bGHpA	JAX 021876	B6;129S-Gt(ROSA)26Sortm66.1(CAG-tdTomato)Hze/J
Ai57(RCFL-Jaws)	Rosa26	pCAG-FSF-LSL-Jaws-GFP-ER2-WPRE-bGHpA		
Ai72(RCL-VSFPB)	Rosa26	pCAG-LSL-VSFP-Butterfly1.2-WPRE-bGHpA		
Ai78(TITL-VSFPB)	TIGRE	pTRE-LSL-VSFP-Butterfly1.2-WPRE-bGHpA	JAX 023528	B6;129S-Igs7tm78.1(tetO-VSFPB1.2)Hze/J
Ai79(TITL-Jaws)	TIGRE	pTRE-LSL-Jaws-GFP-ER2-WPRE-bGHpA	JAX 023529	B6;129S-Igs7tm79.1(tetO-hop/EGFP)Hze/J
Ai82(TITL-GFP)	TIGRE	pTRE-LSL-EGFP-WPRE-bGHpA	JAX 023532	B6;129S-Igs7tm82.1(tetO-EGFP)Hze/J
Ai85(TITL-iGluSnFR)	TIGRE	pTRE-LSL-iGluSnFR-WPRE-bGHpA		
Ai87(RCL-iGluSnFR)	Rosa26	pCAG-LSL-iGluSnFR-WPRE-bGHpA		
Ai92(TITL-YCX2.60)	TIGRE	pTRE-LSL-YCX2.60-WPRE-bGHpA		
Ai93(TITL-GCaMP6f)	TIGRE	pTRE-LSL-GCaMP6f-WPRE-bGHpA	JAX 024103	B6;129S-Igs7tm93.1(tetO-GCaMP6f)Hze/J
Ai94(TITL-GCaMP6s)	TIGRE	pTRE-LSL-GCaMP6s-WPRE-bGHpA	JAX 024104	B6.Cg-Igs7tm94.1(tetO-GCaMP6s)Hze/J
Ai95(RCL-GCaMP6f)	Rosa26	pCAG-LSL-GCaMP6f-WPRE-bGHpA	JAX 024105	B6;129S-Gt(ROSA)26Sortm95.1(CAG-GCaMP6f)Hze/J
Ai96(RCL-GCaMP6s)	Rosa26	pCAG-LSL-GCaMP6s-WPRE-bGHpA	JAX 024106	B6;129S-Gt(ROSA)26Sortm96(CAG-GCaMP6s)Hze/J
Snap25-LSL-2A-GFP	Snap25	Knock-into exon 8: loxP-Stop-loxP-F2A-EGFP	JAX 021879	B6.Cg-Snap25tm1.1Hze/J
Snap25-2A-GCaMP6s	Snap25	Knock-into exon 8: T2A-GCaMP6s	JAX 025111	B6;129S-Snap25tm3.1(GCaMP6s)Hze/J

[a]AIBS: Allen Institute for Brain Science.

Table S2. Other results.

Other tTA Driver Lines[a]	Genomic Target	Testing Results
Pvalb-2A-tTA2	Knock-into 3' UTR: T2A-tTA2	Pvalb-2A-tTA2 mice showed good tTA-induced reporter expression in the first generation of mice, by injection of AAV-pTRE-ChR2-EYFP into the cortex (no TRE promoter driven reporter line was used at the time). But a few generations later, we found that such expression was largely gone throughout the brain and only expression in some cerebellar Purkinje cells was left. ISH using tTA2 riboprobe in the Pvalb-2A-tTA2 mice still showed expected expression pattern of tTA2 mRNA throughout the brain, but there was no induction of reporter gene. AAV-pTRE-ChR2-EYFP injection into the cortex also resulted in no induction.
Sst-tTA2	Knock-into ATG start site: tTA2	Neither tTA2 expression nor induction was observed.
Rorb-IRES-tTA2	Knock-into 3' UTR: IRES2-tTA2	No induction was observed.
Rorb-2A-tTA2	Knock-into 3' UTR: T2A-tTA2	The mouse (F1 generation so far) had beautiful layer 4 specific reporter induction.
Slc32a1-IRES-tTA2	Knock-into 3' UTR: IRES2-tTA2	The mouse (F1 generation so far) had low-level reporter activation in some but not all interneurons.

Other recombinase Driver Lines[b]	Genomic Target	Testing Results
Pvalb-IRES-B3	Knock-into 3' UTR: IRES2-mammalianized B3	No recombination in our Rosa26 double reporter allele bearing recognition sites for B3 and Cre.
Pvalb-IRES-KD	Knock-into 3' UTR: IRES2-mammalianized KD	No recombination in our Rosa26 double reporter allele bearing recognition sites for KD and Cre.

Gal4 Driver Lines[c]	Genomic Target	Testing Results
Thy1-Gal4DBD	Random insertion: Thy1.2 promoter driven Gal4 DNA binding domain	When crossed together with Thy1-VP16AD, the reconstituted Gal4 induced strong expression of GFP from an AAV-based UAS-GFP reporter. However, these double transgenic mice exhibited high mortality rate.
Thy1-mGal4DBD	Random insertion: Thy1.2 promoter driven mammalianized Gal4DBD	When crossed together with Thy1-VP16AD, the reconstituted Gal4 induced strong expression of GFP from an AAV-based UAS-GFP reporter. However, these double transgenic mice exhibited high mortality rate.
Thy1-VP16AD	Random insertion: Thy1.2 promoter driven VP16 activation domain	See above.
Pvalb-2A-Gal4	Knock-into 3' UTR: T2A-Gal4	To examine Gal4 expression at an intermediate expression level, we generated Pvalb-2A-Gal4 knock-in mice. The germline transmitted mice again exhibited high mortality rate at ~3-4 postnatal weeks. These results indicate that the Gal4 gene may be toxic in the adult mouse brain. Thus, further testing of this approach was terminated.

[a]In an effort to expand the repertoire of cell type specific tTA driver lines, we generated and tested 5 knock-in tTA lines using the optimized tTA2 version (Urlinger et al., 2000). The testing results are shown here.

[b]We tested the intersection between Cre and two other recombinases, KD and B3, with negative outcomes, although KD and B3 work well to regulate expression in *Drosophila* and have been reported as having activity in mammalian cells (Nern et al., 2011).

[c]The yeast Gal4/UAS system was first introduced in mice as a binary expression system (Ornitz et al., 1991). It has been widely used in *Drosophila* for cell-specific gene expression (Jenett et al., 2012), and a split-Gal4 system has been developed as an intersectional strategy in *Drosophila* (Luan et al., 2006). However, the literature reports limited use of Gal4 in the mouse brain, and then only during neural development in juvenile mice (Hu et al., 2004; Rowitch et al., 1999). As part of our evaluation of various intersectional approaches, we generated Thy1.2 promoter (Caroni, 1997) driven transgenic lines expressing split-Gal4 components (i.e. Gal4-DBD, AD-VP16) (Luan et al., 2006), and knock-in line expressing Gal4 in the *Pvalb* locus. The testing results are shown here.

Movie S1. Two-Photon imaging at 120 μm below the pia in visual cortex of an Emx1-IRES-Cre;Ai95(RCL-GCaMP6f) mouse, matching dataset used in **Figure 7D**. (Related to **Figure 7**.) Visual stimuli were presented to the mouse during the data acquisition period.

Movie S2. Two-Photon imaging at 300 μm below the pia in visual cortex of an Emx1-IRES-Cre;Ai95(RCL-GCaMP6f) mouse, matching dataset used in **Figure 7D**. (Related to **Figure 7**.) Visual stimuli were presented to the mouse during the data acquisition period.

Movie S3. Two-Photon imaging at 120 μm below the pia in visual cortex of an Emx1-IRES-Cre;Camk2a-tTA;Ai93(TITL-GCaMP6f) mouse, matching dataset used in **Figure 7E**. (Related to **Figure 7**.) Visual stimuli were presented to the mouse during the data acquisition period.

Movie S4. Two-Photon imaging at 300 μm below the pia in visual cortex of an Emx1-IRES-Cre;Camk2a-tTA;Ai93(TITL-GCaMP6f) mouse, matching dataset used in **Figure 7E**. (Related to **Figure 7**.) Visual stimuli were presented to the mouse during the data acquisition period.

SUPPLEMENTAL EXPERIMENTAL PROCEDURES

Transgenic mice generation

Targeting constructs were generated using a combination of molecular cloning, gene synthesis (GenScript, Piscataway, US) and Red/ET recombineering (Gene Bridges, Heidelberg, DE). Coding sequences for the fluorescent proteins and optogenetic tools included in the Ai reporter lines listed in **Table 1** were cloned between the LSL cassette and the WPRE element in the targeting backbones described below, either directly from acquired plasmids or after gene synthesis based on published information. The 129S6B6F1 ES cell line, G4, was used to generate all transgenic mice by homologous recombination and, in many cases, subsequent Flp- recombinase-mediated cassette exchange (RMCE). Correct clones were used in blastocyst injections to obtain germline transmission. Resulting mice were crossed to the Rosa26-PhiC31 mice (JAX Stock # 007743) to delete the pPGK-neo or pPGK-hygro selection marker cassette, and then backcrossed to C57BL/6J mice and maintained in C57BL/6J congenic background.

Rosa26-pCAG-LSL-WPRE-bGHpA (RCL) vectors: Vector backbone has been previously described (Madisen et al., 2010) and contains a loxP – stop codons – 3x SV40 polyA – loxP cassette.

Rosa26-pCAG-FSF-LSL-WPRE-bGHpA (RCFL) and Rosa26-RSR-LSL-WPRE-bGHpA (RCRL) vectors: The original Rosa26 targeting vector above was modified to include an additional stop cassette between the CAG promoter and the loxP – stop codons – 3x SV40 polyA – loxP unit. The additional stop cassettes contained: FRT (or Rox) – an 8 amino acid open reading frame – stop codons – a synthetic polyA – hGH polyA – TK polyA – FRT (or Rox). Note that the new stop cassette in FSF and RSR is different from the previously created stop cassette in LSL, to reduce the sequence repetitiveness in the new targeting vectors.

TIGRE vectors: As shown in **Figure S1B**, ES clones carrying TIGRE reporters were generated by a recombinase-mediated cassette exchange (RMCE) strategy into an ES clone that had been first targeted with a Flp/FRT-based docking site. In our first step to generate this ES clone with a docking site inserted into the TIGRE locus, the original targeting vector contained: 5' and 3'homology arms (base pairs 21539059-21545314 and 21545315-21549209, respectively, of ref_NC 000075.6 on mouse chromosome 9) flanking the following cassette: FRT3 (F3) – AttB – pPGK – neomycin-resistant gene – PGK polyA – FRT5 (F5) – mRNA splice acceptor – domain 2 from the hygromycin-resistant gene – SV40 polyA – AttP. Southern blot analysis was done on neo resistant ES clones to confirm correct construct integration. Several targeted clones were injected into blastocysts, and those that gave rise to high-percentage chimeras were chosen for expansion and use in the RMCE transfections.

Replacement vectors used for RMCE into the TIGRE docking site: The replacement vectors were in the following configuration (**Fig. S1B**): F3 – 2 copies of the 1.2-kb chicken β-globin HS4 insulator fragment – pTRE-Tight – loxP – an 8 amino acid open reading frame – stop codons – a synthetic polyA – hGH polyA – PGK polyA – loxP – Transgene – WPRE – bGH polyA – 2 copies of the 1.2-kb chicken β-globin HS4 insulator fragment – AttB – pPGK – domain 1 from the hygromycin-resistant gene – mRNA splice donor – F5. The TRE promoter used here was from Clontech's pTRE-Tight vector, which contains a modified Tet response element (TREmod) that consists of seven direct repeats of a 36-bp sequence containing the 19-bp tet operator sequence (tetO); the TREmod is just upstream of the minimal CMV promoter. Supercoiled replacement vectors were co-transfected with a pCAG-Flpe plasmid into the above TIGRE docking clones and selected with hygromycin. Resistant colonies were screened for correct 5' and 3' junctions and for the lack of the original docking site sequence. The general configuration of the replacement vector was modified to generate the Ai118 line (**Fig. S6**), in which the TRE-pCMVmin promoter was replaced by the CAG promoter present in all Rosa26 reporter constructs.

Pvalb-targeted vectors: The *Pvalb* locus was originally targeted with homologous recombination to insert T2A-Cre at the endogenous stop codon (Madisen et al., 2010), using a targeting vector containing the following components (**Fig. S1A**): 5' arm – F3 – last ~250bp of intron 3 – exon 4 up to the endogenous stop codon – T2A-Cre – stop codon – Pvalb 3' UTR – AttB – pPGK – neomycin-resistant gene – PGKpA – F5 – mRNA splice acceptor – domain 2 from the hygromycin-resistant gene – SV40 polyA – AttP – 3' arm. Correctly targeted neomycin resistant clones were identified by PCR, and then confirmed by Southern blot. One clone that gave high percentage chimeras following blastocyst injection was used in subsequent RMCE experiments. Replacement vectors included: F3 – last ~250bp of intron 3 – exon 4 up to the endogenous stop codon – T2A-Transgene (Flpe/Flpo/Dre) – stop codon – Pvalb 3' UTR – AttB – pPGK – domain 1 from the hygromycin-

resistant gene – mRNA splice donor – F5. Following co-transfection with a pCAG-Flpe plasmid, hygromycin resistant colonies were screened for correct 5' and 3' junctions and for lack of the original vector sequence.
Snap25-targeted vectors: The *Snap25* locus was targeted with homologous recombination to insert LSL-F2A-GFP at the endogenous stop codon, using a targeting vector containing the following components: 5' arm – F3 – last ~300bp of intron 7 – exon 8 up to the endogenous stop codon – loxP – stop codons – PGK polyA – loxP – F2A – EGFP – WPRE – bGH polyA – AttB – pPGK – neomycin-resistant gene – PGKpA – F5 – mRNA splice acceptor – domain 2 from the hygromycin-resistant gene – SV40 polyA – AttP – 3' arm. Correctly targeted neomycin resistant clones were identified by PCR, and then confirmed by Southern blot. One clone that gave high percentage chimeras following blastocyst injection was used in a RMCE transfection to switch the LSL-F2A-GFP expression unit for a T2A-GCaMP6s expression unit. The replacement vector included: F3 – last ~250bp of intron 7 – exon 8 up to the endogenous stop codon – T2A-GCaMP6s – WPRE – bGH polyA – AttB – pPGK – domain 1 from the hygromycin-resistant gene – mRNA splice donor – F5. Following co-transfection with a pCAG-Flpe plasmid, hygromycin resistant colonies were screened for correct 5' and 3' junctions and for lack of the original vector sequence.
Nr4a2-SA-IRES-Dre vector: Targeted mice were generated in collaboration with the NorCOMM high throughput gene targeting project (http://www.norcomm.org/index.htm). The *Nr4a2* locus was targeted with a vector that results in deletion of the protein encoding sequence and replacement with an F3 – mRNA splice acceptor – IRES-Dre – FRT cassette. A mammalian codon-optimized Dre was used here.
Rasgrf2-targeted vector: The *Rasgrf2* locus was targeted with homologous recombination to insert T2A-dCre at the endogenous stop codon, using a targeting vector containing the following components: 5' arm – F3 – last ~300bp of intron 33 – exon 34 up to the endogenous stop codon – T2A-dCre – bGH polyA – AttB – pPGK – neomycin-resistant gene – PGKpA – F5 – mRNA splice acceptor – domain 2 from the hygromycin-resistant gene – SV40 polyA – AttP – 3' arm. The dCre fusion gene (also called destabilized Cre, hDHFR/Cre or ecDHFRR12Y/Y100I/Cre) is Cre recombinase fused at its N-terminus to the first 159 amino acids of the *E. coli* K-12 dihydrofolate reductase gene, harboring G67S and R12Y/Y100I destabilizing domain mutations (Sando et al., 2013). Activity of dCre recombinase is low in the absence of trimethoprim (TMP), and full Cre activity was induced in these mice by an intraperitoneal (IP) injection of TMP at 0.25 mg/g body weight per day for 3 days. Since TMP has low solubility in aqueous solution, 10x stock solution in 100% DMSO needs to be quickly diluted with 0.9% saline and immediately (within 1 min) injected into mice. Alternatively, TMP can be diluted from a 10x stock in 100% DMSO with a 2% methylcellulose solution and administered via oral gavage (PO) at 0.3 mg/g body weight per day for 3 days. Mice can be used for experiments starting at 1-2 weeks after dosing.

Transgenic mice expression characterization
Driver and reporter lines were crossed together according to specific schemes. Expression of the reporter genes was assessed by native fluorescence (without antibody staining) on perfused, microtomed sections or by *in situ* hybridization (ISH) on fresh-frozen sections.
For analysis of native fluorescence, animals were perfused with 4% paraformaldehyde (PFA) in 0.1 M PB. Brains were fixed for an additional 18 hr at 4°C, then cryoprotected in 10% sucrose in PBS at 4°C overnight. Brains were sectioned to 100 µm using a Leica SM2000R sliding microtome and sections were mounted onto slides. The sections were examined by epifluorescence microscopy without antibody staining. For confocal imaging, sections were imaged using an Olympus FV1000 confocal system with 10x or 20x objectives. To keep imaging conditions constant for comparison purposes, laser power was always set at 10%, whereas PMT gain was adjusted to stay within proper dynamic range but kept constant within each group of brains being compared and the value was reported for each confocal image shown in this paper.
For FACS sorting and quantification of fluorescence level, single cell suspensions of live cells were analyzed for mean fluorescence intensity on a BD FACSAria II SORP instrument using settings optimized for side and forward scatter. Wild-type cells were used as a negative control, and doublets, debris and DAPI+ dead cells were gated out. Graphics were done with FloJo.
For ISH, we used the Allen Institute–established pipelines for tissue processing, riboprobe hybridization, image acquisition and data processing (Lein et al., 2007; Madisen et al., 2010). Riboprobes used for expression profiling ISH were designed against Cre, tdTomato and EYFP/EGFP. All transgenic mice ISH data can be found at the Transgenic Characterization database (http://connectivity.brain-map.org/transgenic/search/basic) (Harris et al., 2014).

Hippocampal slice recording of VSFP activities

We prepared acute coronal slices (300 μm thick) containing cortex and hippocampus (vibratome VTS1000S, Leica). The mice (2-3 months old) were sedated by exposure to CO_2 gas, decapitated, the brain immediately removed and submerged in ice-cold cutting solution (in mM: 87 NaCl, 75 sucrose, 2.5 KCl, 6 $MgCl_2$, 0.5 $CaCl_2$, 25 Glucose, 25 $NaHCO_3$, 1.25 NaH_2PO_4) saturated with 95% O_2 and 5% CO_2. The slices were transferred to artificial cerebrospinal fluid (ACSF) containing (in mM) 126 NaCl, 3 KCl, 1 NaH_2PO_4, 2 $MgSO_4$, 2 $CaCl_2$, 25 $NaHCO_3$, 15 glucose, saturated with 95% O_2 and 5% CO_2, and maintained initially at 35ºC for 30 min and then at room temperature for at least another 30 min before recording.

Slices were transferred to the recording chamber of an upright microscope (Eclipse FN1, Nikon). The dentate gyrus was imaged with a 16× water immersion objective (Nikon) using fluorescence excitation (mCitrine, 483/32-25, Semrock FF01) from a halogen lamp (Moritex Corporation, Japan) and emission (542/27-25 for mCitrine, Semrock FF01; and 594R-25 for mKate, Semrock BLP01) collected with a cooled CCD camera (Hamamatsu C-9100), at 118 Hz (4× binning) Simple PCI (Hamamatsu Corporation, Japan). Electrical synaptic stimulation was synchronized with a Master 8 (A.M.P.I., Israel) and used an ACSF-filled glass electrode (approximately 1 MΩ) placed in the middle of the molecular layer approximately 200-400 μm from the recording region of interest (ROI). Fluorescence signals from a single ROI placed in the molecular layer of the dentate gyrus were bleach corrected by subtracting stimulated responses from non-stimulated responses, both averaged 3-5 times, using Excel.

***In vivo* wide-field voltage imaging**

Six mice were imaged repeatedly between the ages of 3 to 9 months. The mice were implanted with a head plate and an 8 mm circular window for imaging through thinned skull, as described elsewhere (Drew et al., 2010). During imaging experiments, the animal was placed on a spherical treadmill, where it was allowed to move freely while its head was held fixed for imaging. To excite the donor fluorophore (mCitrine), we diverted a blue LED light (LEX2-B, Brainvision Inc.) onto the cortex via a dichroic mirror (FF506-Di03, Semrock Inc.). To acquire both fluorophores we used two sCMOS cameras (pco.edge, PCO AG). The first camera recorded the emitted fluorescence from mCitrine, which was reflected by a second dichroic mirror (FF593-Di03, Semrock Inc.), passed through an emission filter (FF01-543/50-25, Semrock Inc.). The second camera recorded the emitted fluorescence from mKate2, passed through the second dichroic mirror and an emission filter (BLP01-594R-25, Semrock Inc.). These cameras were controlled by an external TTL pulse synchronized with the sensory stimulation. The image acquisition rate was 50 Hz, with a nominal spatial resolution of 123 pixels/mm.

Stimuli were trains of visual, somatosensory, or auditory stimuli, delivered to elicit periodic responses in cortex. Stimulus trains were typically presented for 5 s and repeated 20 times for each modality. For retinotopy mapping, 4 different positions and the no-stimulus condition were randomized. For somatosensory and auditory mapping, air puff, sham of air puff, auditory tone, and the no-stimulus conditions were randomized. Visual stimuli were presented via LCD monitors placed 20-30 cm away from the animal. Horizontal or vertical contrast-reversing bars or gratings were presented inside a rectangular window (reversal frequency 2 Hz, spatial frequency 0.03 cycles/deg). These stimuli elicit cortical responses at twice the reversal frequency (4 Hz). To measure preferred azimuth, the rectangular window was 60° high and 20° wide. To measure preferred elevation, it was 15° high and 60° wide. Somatosensory stimuli were trains of air puffs delivered from a spritzer (Pressure system IIe, Toohey Company) towards the whiskers at a pressure of 20 PSI via silicone tube (0.5 mm open tip diameter). Air puffs lasted 20 ms and were repeated at 4 Hz. To control for the effect of the sound, sham air puffs were randomly interleaved and delivered away from the whiskers. Auditory stimuli were trains of tones delivered at 80 dB_{SPL} via a magnetic speaker (Tucker-Davis Technologies) placed 15 cm in front of the animal. Each tone lasted 50 ms, and was repeated at 6 Hz. Tones of different frequencies were randomly interleaved.

To eliminate slow (hemodynamic) components of the optical signals, image sequences were high-pass filtered with a causal Butterworth filter (0.5 Hz corner frequency). The image sequences were then normalized by the data during prestimulus period. The voltage signal was calculated as the ratio of acceptor and donor signals from the two cameras, after aligning them (with Matlab's Image Processing Toolbox) and equalizing fluctuation at the heartbeat frequency (Akemann et al., 2012). We then averaged the images across repeats, and measured the amplitude of the oscillation of each pixel at the response frequency (4 Hz for visual stimuli and air puffs, 6 Hz for tones). We then smoothed the resulting maps with a Gaussian filter (sigma = 97 μm). The map of retinotopy was estimated by fitting the response amplitudes for different stimulus positions (azimuth or elevation) with a

Gaussian function. The width of the Gaussian function (sigma) was estimated as a global parameter across pixels. To obtain the map of tonotopy, the same algorithm was applied to the response amplitudes for different tone frequencies. To calculate signal-to-noise ratio during visual stimulation, we took the responses to a vertical flickering bar presented to the monocular zone. We obtained a map of signal-to-noise ratio (S/N) as the 4 Hz amplitude during the stimulation (averaged over 12 trials), divided by the 4 Hz amplitude during no-stimulation. To estimate S/N for each animal, we picked all the pixels within 0.5 mm from the pixel that showed the highest signal, and averaged the S/N over those pixels.

***In vivo* two-photon calcium imaging in GCaMP6 mice**

Each mouse received surgery for head-plate implantation and a craniotomy for glass window placement over visual cortex starting at age P45. A metal head-plate was cemented to the skull and a 5 mm circular craniotomy was made. Two 5 mm and one 8 mm circular glass cover slips were glued together and fitted into the craniotomy. The 8 mm coverslip rested against the surface of the skull and was cemented in place. Mice were allowed 7 days to recover from surgery and were then habituated to head fixation and the experimental set-up including visual stimuli for 5 to 14 days depending on the temperament of the mouse.

During experiments, the animal was permitted to run on a freely-rotating disc while visual stimuli were presented to the eye contralateral to the imaged region. Visual stimuli and software for tracking motion of the mouse were created in Python. Stimuli consisted of drifting sinusoidal gratings presented at 80% contrast shown in random order for all permutations of 5 spatial frequencies (SF), 5 temporal frequencies (TF), and 8 orientations (0° to 315° in 45° steps). Stimuli were presented 8 times each, full-field, for 3 seconds with a mean luminance inter-stimulus-interval of 2 seconds on an LCD monitor spanning 60° in elevation and 130° in azimuth. The mouse's eye was positioned 22 cm away from the center of the monitor.

Image data were acquired using a custom built two-photon microscope with resonant scanners, and a MaiTai femtosecond laser (Spectra-Physics) at 920 nm through a 16x water-immersion objective lens (Nikon, NA 0.8). Images were collected at approximately 30 Hz with 512 lines per frame. Laser powers (at objective) used were 100 mW (at 120 μm depth) and 130 mW (at 300 μm depth) for Ai95 mice, 90 mW (at 120 μm depth) and 120 mW (at 300 μm depth) for Ai93 mice. Data analysis was performed in Python and Matlab. In summary, data was down-sampled to 4 Hz and motion corrected using cross-correlation between frames. Segmentation was achieved by either using Independent Component Analysis (ICA) followed by automated Region of Interest (ROI) selection or by manually selection of ROIs, and traces were extracted by averaging all pixels in a segment and measuring their fluorescence over time. The background for $\Delta F/F$ calculation was determined using a sliding window to find a local minimum for fluorescence for the duration of the experiment. Tuning was calculated from the averaged response over the full 3 seconds of stimulus presentation.

***In vivo* two-photon calcium imaging in YCX2.60 mice**

Adult mice (>P45) were implanted with a 3-mm cranial window above the barrel field in somatosensory cortex and a head post. YCX2.60 expression was induced by i.p. injection of Trimethoprim (TMP) one week before imaging (dissolved in DMSO and diluted with saline; dosage: 150 μg/g body weight).

Mice were anesthetized with 0.5-0.8% isofluorane and body temperature was maintained at 37ºC with a heating blanket. We identified the barrel column corresponding to the C2 whisker using intrinsic optical imaging. The C2 whisker was stimulated with a piezoelectric element (2º amplitude in the rostrocaudal direction at 10 Hz) and reflectance images were acquired with red light illumination of the cortical surface (630-nm light-emitting diode, LED). Images were collected through a 4x objective with a CCD camera (Toshiba TELI CS3960DCL; 12-bit; 3-pixel binning, 427x347 binned pixels, 8.6 μm pixel size, 10 Hz frame rate). The intrinsic signal of the C2 barrel column was mapped to the blood vessel reference image, which was obtained with green light illumination (546-nm LED).

Two-photon calcium imaging of somatosensory cortex was performed with a custom-built two-photon microscope using galvanometric scanners and a Ti:sapphire laser system (Mai Tai Deep See; Newport Spectra-Physics). Fluorescence images of 128x64 pixels were acquired at 15 Hz through a 16x water-immersion objective lens (Nikon, NA 0.8). YCX2.60 fluorescence excited at 840-nm wavelength with 40 mW laser power after objective was collected in two spectral channels using blue (480/60 nm) and yellow (542/50 nm) emission filters. ROIs of active cells were manually annotated, and fluorescence traces were extracted by subtracting background and averaging all ROI pixels for each channel (CFP and YFP, respectively). The ratio R was calculated as the

ratio of the YFP and the CFP signals. Fluorescence traces were also expressed as relative percentage changes $\Delta R/R = (R-R_0)/R_0$ with the baseline ratio R_0 determined as the bottom 10^{th} percentile of the ratio trace.
For *in vitro* measurements of yellow cameleon properties, 3 days after transfection using Lipofectamine 2000 (Invitrogen), HeLa cells expressing YC2.60 or YCX2.60 were imaged on an inverted microscope (IX73, Olympus) with a dual CCD camera (ORCA-D2, Hamamatsu). A 440DF20 excitation filter, a 455DRLP dichroic mirror and optical block A11400-03 in ORCA-D2 (dichroic mirror 510 nm, 483/32 nm for CFP, 542/27 nm for YFP) were used for dual-emission imaging. The sequence for YCX2.60 has been deposited in the DDBJ/EMBL/GenBank databases (accession number LC025957).

***In vitro* and *in vivo* electrophysiology of optogenetic silencing**
All light powers were measured with a PM200B photodetector (Thorlabs); all *in vivo* light powers were reported as measured at a 200-μm fiber tip with an integrating sphere (S142C, Thorlabs) rather than calculated at a distance away from the fiber (Chuong et al., 2014).
In vivo extracellular recordings were conducted as before (Chuong et al., 2014). Briefly, adult (2-7 months old) mice were implanted with a metal headplate and a circular craniotomy was made over the primary visual cortex. Extracellular recordings were conducted in the cortex of awake, head-fixed mice using 3-10 MΩ saline-filled glass microelectrodes containing silver/silver-chloride electrodes. Signals were amplified with a Multiclamp 700B and digitized with a Digidata 1440B, using pClamp software (Molecular Devices). A recording glass electrode was attached to a 200-μm diameter optical fiber, coupled to a 637 nm laser (Coherent Lasers), such that the fiber tip was 500 ± 50 μm above the tip of the electrode, and guided into the brain with a Sutter manipulator. Light pulses were controlled via Digidata-generated TTL pulses, and data was analyzed using MATLAB and Offline Sorter (Plexon). Light-modulated units were identified by performing a paired t-test between the 5-s illumination period and the baseline firing period of the same time duration immediately before illumination, thresholding at $P < 0.05$. The degree of suppression was calculated for each cell by dividing the mean firing rate during the light stimulus by the mean baseline firing rate during the same time duration before light stimulation onset.
Ex vivo electrophysiology was carried out with 300-μm brain slices. Mice (2-7 months old) were deeply anaesthetized with isoflurane, then transcardially perfused with 40 ml of ice-cold ACSF (in mM: NaCl 87, KCl 2.5, NaH_2PO4 1.3, $MgCl_2$ 7, $NaHCO_3$ 25, sucrose 75, ascorbate 5, $CaCl_2$ 0.5, in ddH_2O; 320-330 mOsm, pH 7.30-7.40, saturated with 95% O_2 / 5% CO_2). The brain was sectioned using a Compresstome (Precisionary Instruments Inc.) and slices were incubated in ACSF (containing in mM: NaCl 124, KCl 2.5, NaH_2PO4 1.25, $MgSO_4$ 1, $NaHCO_3$ 25, sodium pyruvate 3, sodium L-ascorbate 0.5, myo-inositol 3, taurine 0.01, glucose 10, $CaCl_2$ 1.2, in ddH_2O; 299-301 mOsm; pH 7.35-7.45, saturated with 95% O_2 / 5% CO_2) at 32°C for ≥ 90 min before being transferred to the recording chamber for electrophysiology. Once in the recording chamber, slices were continuously perfused at a rate of 2 ml/min with fully oxygenated ACSF at 32°C with added Picrotoxin (100 μM) and kynurenic acid (1 mM) to block GABAergic and glutamatergic synaptic transmission. Neurons were identified under DIC based on pyramidal morphology rather than fluorescence and optical activation with 500-ms light pulses was delivered using 530 or 625 nm LEDs (Thorlabs). The 625 nm LED was additionally filtered with a 632 nm ± 11 nm filter (Semrock). 4–6 MΩ borosilicate glass pipettes (Kings Precision Glass) filled with internal solution (containing (in mM): potassium gluconate 120, KCl 7, EGTA 1, HEPES 10, Mg-ATP 3, Na-GTP 0.4, phosphocreatine 10; 290 mOsm; pH 7.3) were used for whole-cell patch-clamp recording in slice. During recording, membrane capacitance (Cm), series resistance (Rs) and input resistance (Rin) were frequently monitored. Cells with Vrest > −60 mV, Rs > 30 MΩ or Rs/Rin changed over 30% during recording were excluded from final data analysis.

SUPPLEMENTAL REFERENCES

Akemann, W., Mutoh, H., Perron, A., Park, Y.K., Iwamoto, Y., and Knopfel, T. (2012). Imaging neural circuit dynamics with a voltage-sensitive fluorescent protein. J. Neurophysiol. *108*, 2323-2337.
Caroni, P. (1997). Overexpression of growth-associated proteins in the neurons of adult transgenic mice. J Neurosci Methods *71*, 3-9.
Chuong, A.S., Miri, M.L., Busskamp, V., Matthews, G.A., Acker, L.C., Sorensen, A.T., Young, A., Klapoetke, N.C., Henninger, M.A., Kodandaramaiah, S.B.*, et al.* (2014). Noninvasive optical inhibition with a red-shifted microbial rhodopsin. Nat. Neurosci. *17*, 1123-1129.
Drew, P.J., Shih, A.Y., Driscoll, J.D., Knutsen, P.M., Blinder, P., Davalos, D., Akassoglou, K., Tsai, P.S., and Kleinfeld, D. (2010). Chronic optical access through a polished and reinforced thinned skull. Nat. Methods *7*, 981-984.
Harris, J.A., Hirokawa, K.E., Sorensen, S.A., Gu, H., Mills, M., Ng, L.L., Bohn, P., Mortrud, M., Ouellette, B., Kidney, J.*, et al.* (2014). Anatomical characterization of Cre driver mice for neural circuit mapping and manipulation. Front. Neural Circuits *8*, 76.
Hu, Q., Ueno, N., and Behringer, R.R. (2004). Restriction of BMP4 activity domains in the developing neural tube of the mouse embryo. EMBO Rep *5*, 734-739.
Jenett, A., Rubin, G.M., Ngo, T.T., Shepherd, D., Murphy, C., Dionne, H., Pfeiffer, B.D., Cavallaro, A., Hall, D., Jeter, J.*, et al.* (2012). A GAL4-driver line resource for Drosophila neurobiology. Cell Rep *2*, 991-1001.
Lein, E.S., Hawrylycz, M.J., Ao, N., Ayres, M., Bensinger, A., Bernard, A., Boe, A.F., Boguski, M.S., Brockway, K.S., Byrnes, E.J.*, et al.* (2007). Genome-wide atlas of gene expression in the adult mouse brain. Nature *445*, 168-176.
Luan, H., Peabody, N.C., Vinson, C.R., and White, B.H. (2006). Refined spatial manipulation of neuronal function by combinatorial restriction of transgene expression. Neuron *52*, 425-436.
Madisen, L., Zwingman, T.A., Sunkin, S.M., Oh, S.W., Zariwala, H.A., Gu, H., Ng, L.L., Palmiter, R.D., Hawrylycz, M.J., Jones, A.R.*, et al.* (2010). A robust and high-throughput Cre reporting and characterization system for the whole mouse brain. Nat. Neurosci. *13*, 133-140.
Nern, A., Pfeiffer, B.D., Svoboda, K., and Rubin, G.M. (2011). Multiple new site-specific recombinases for use in manipulating animal genomes. Proc. Natl. Acad. Sci. USA *108*, 14198-14203.
Ornitz, D.M., Moreadith, R.W., and Leder, P. (1991). Binary system for regulating transgene expression in mice: targeting int-2 gene expression with yeast GAL4/UAS control elements. Proc. Natl. Acad. Sci. USA *88*, 698-702.
Rowitch, D.H., B, S.J., Lee, S.M., Flax, J.D., Snyder, E.Y., and McMahon, A.P. (1999). Sonic hedgehog regulates proliferation and inhibits differentiation of CNS precursor cells. J. Neurosci. *19*, 8954-8965.
Sando, R., 3rd, Baumgaertel, K., Pieraut, S., Torabi-Rander, N., Wandless, T.J., Mayford, M., and Maximov, A. (2013). Inducible control of gene expression with destabilized Cre. Nat. Methods *10*, 1085-1088.
Urlinger, S., Baron, U., Thellmann, M., Hasan, M.T., Bujard, H., and Hillen, W. (2000). Exploring the sequence space for tetracycline-dependent transcriptional activators: novel mutations yield expanded range and sensitivity. Proc. Natl. Acad. Sci. USA *97*, 7963-7968.